2D TWO-LAYER SHALLOW-WATER MODEL WITH A BANK-FAILURE OPERATOR FOR DAM-BREAK WAVES ON MOBILE BEDS

Catherine Swartenbroekx[1], Yves Zech[2], & Sandra Soares-Frazão[2]

[1]Fonds de la Recherche Scientifique – FNRS & Civil and Environmental Engineering, Institute of Mechanics, Material and Civil Engineering, Université catholique de Louvain, Belgium, Place du Levant 1, B-1348 Louvain-la-Neuve

[2]Civil and Environmental Engineering, Institute of Mechanics, Material and Civil Engineering, Université catholique de Louvain, Belgium, Place du Levant 1, B-1348 Louvain-la-Neuve

E-mail: catherine.swartenbroekx@uclouvain.be, yves.zech@uclouvain.be, sandra.soares-frazao@uclouvain.be

Abstract

To consider both bed and bank erosion due to a dam-break induced wave, a bank-failure operator is inserted into a two-dimensional (2D) two-layer shallow-water model. This model accounts explicitly for the inertia of the bed-load transport, considering an upper layer made of clear water and a lower layer, called the bed-load transport layer, made of a mixture of water and moving grains. These layers flow on a motionless bed and are assumed to present distinct depth-averaged velocities. The model accounts for the grain entrainment across the bed interface and for the mass and momentum exchanges between the flowing layers thanks to the definition of an erosion rate. This shallow-water model is solved by a first-order finite-volume scheme on an unstructured triangular mesh. The bank-failure operator consists in comparing locally for each computational cell the bed inclination to the sediment stability angles, considering the impact of a water-level rise as a destabilizing phenomenon. After an erosion or deposition update due to the bed-load transport, the unstable bed elements are tilted around an appropriate axis of rotation, ensuring mass conservation of the assumed homogeneous material. The numerical model is tested for a collapsing circular hole and against laboratory tests of a dam-break flow; firstly in a prismatic channel made of coarse sand, and then over an initial bed step.

Introduction

The dam breaks constitute a danger for the surrounding inhabitants and infrastructures. To design appropriate emergency plans and reduce the risk posed by these dams, the time and space evolution of the consequences must be known for these potential failures. The geomorphic consequences of a dam-break induced wave on a mobile bed are governed by bed and bank erosion. To consider both erosion mechanisms, a bank-failure operator is inserted into a two-dimensional (2D) two-layer shallow-water model. This model has the advantage to account explicitly for the inertia of the bed-load transport and, doing so, to be able to treat intense sediment transport due to fast transient flows.

Two-layer model with bank-failure operator

The two-layer description considers an upper layer made of clear water and a lower layer, called the bed-load transport layer, made of a mixture of water and moving grains (Zech et al. 2009). These layers flow on a motionless bed and present distinct depth-averaged velocities $\mathbf{u}_w$ and $\mathbf{u}_s$. It is also assumed that the transport layer and the motionless bed present distinct sediment concentrations C_s and C_b, which are kept constant all along the flow (Figure 1).

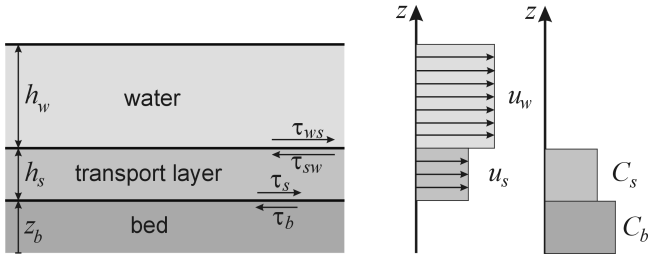

Figure 1: The two-layer model, where z_b is the bed level, h_s the transport layer thickness, h_w the clear-water layer thickness, τ_{ws}, τ_{sw}, τ_s, τ_b the shear stresses.

Governing equations of the 2D two-layer model

The model accounts for the grain entrainment across the bed interface and for the mass and momentum exchanges between the flowing layers thanks to the definition of an erosion rate:

$$e_b = -\frac{\partial z_b}{\partial t} \tag{1}$$

This erosion rate is positive in case of erosion and negative in case of deposition. It depends on the shear stresses τ_s and τ_b on both sides of the bed interface (Zech et al. 2009):

$$e_b = \frac{\|\boldsymbol{\tau}_s\| - \|\boldsymbol{\tau}_b\|}{\rho_b' \|\mathbf{u}_s\|} \tag{2}$$

These shear stresses are driven by Chezy-like and Mohr-Coulomb closure equations, respectively:

$$\boldsymbol{\tau}_{ws} = \rho_w C_{f,w} \|\mathbf{u}_r\| \mathbf{u}_r \tag{3}$$

$$\boldsymbol{\tau}_s = \rho_s' C_{f,s} \|\mathbf{u}_s\| \mathbf{u}_s \tag{4}$$

$$\boldsymbol{\tau}_b = \left(\tau_{crit} + tg\varphi(\rho_s' - \rho_w) g h_s\right) \frac{\mathbf{u}_s}{\|\mathbf{u}_s\|} \tag{5}$$

where ρ_w, ρ_s' and ρ_b' are the densities of the clear water, of the bed-load transport layer and of the bed, respectively; $\rho_s' = (1-C_s)\,\rho_w + C_s\,\rho_s$, $\rho_b' = (1-C_b)\,\rho_w + C_b\,\rho_s$, where ρ_s is the granular density; $C_{f,w}$ and $C_{f,w}$ are the friction coefficients; $\mathbf{u}_r = \mathbf{u}_w - \mathbf{u}_s$ is the relative velocity; τ_{crit} is the critical shear stress, φ the angle of repose and g the gravity acceleration.

In a same way, the rate e_s is defined and related to the time evolution $-\partial z_s/\partial t$ of the interface between the two layers. Distinct depth-averaged granular concentrations are assumed in the bed-load layer and in the motionless bed (Figure 1). This assumption allows the required expansion of sediments leaving the bed layer to be mobilized during erosion and the compaction of deposed sediments. The sediment transfer from the motionless bed to the transport layer does not affect the water level z_w but well the top level z_s of the bed-load transport layer and the bed level z_b. The continuity of these vertical exchanges leads to a relation between both erosion rates e_b and e_s of opposite signs (Zech et al. 2009):

$$e_s = -\frac{C_b - C_s}{C_s} e_b \tag{6}$$

Equation (1) is considered as the first equation of the system. To complete this system, the continuity equations (7) and (8) and the 2D momentum conservation equations (9-12) are written for each layer:

$$\frac{\partial h_w}{\partial t} + \frac{\partial q_{wx}}{\partial x} + \frac{\partial q_{wy}}{\partial y} = e_s \tag{7}$$

$$\frac{\partial h_s}{\partial t} + \frac{\partial q_{sx}}{\partial x} + \frac{\partial q_{sy}}{\partial y} = e_b - e_s \tag{8}$$

$$\frac{\partial q_{wx}}{\partial t} + \frac{\partial}{\partial x}\left(\frac{q_{wx}^2}{h_w} + \frac{1}{2} g h_w^2\right) + \frac{\partial}{\partial y}\left(\frac{q_{wx} q_{wy}}{h_w}\right) = -g h_w \frac{\partial z_s}{\partial x} + u_{wx} e_s - \frac{\tau_{wsx}}{\rho_w} \tag{9}$$

$$\frac{\partial q_{wy}}{\partial t} + \frac{\partial}{\partial x}\left(\frac{q_{wx} q_{wy}}{h_w}\right) + \frac{\partial}{\partial y}\left(\frac{q_{wy}^2}{h_w} + \frac{1}{2} g h_w^2\right) = -g h_w \frac{\partial z_s}{\partial y} + u_{wy} e_s - \frac{\tau_{wsy}}{\rho_w} \tag{10}$$

$$\frac{\partial q_{sx}}{\partial t} + \frac{\partial}{\partial x}\left(\frac{q_{sx}^2}{h_s} + \frac{1}{2} g h_s^2 + g\chi h_w h_s\right) + \frac{\partial}{\partial y}\left(\frac{q_{sx} q_{sy}}{h_s}\right) = g\chi h_w \frac{\partial z_s}{\partial x} - g(\chi h_w + h_s)\frac{\partial z_b}{\partial x} - \chi u_{wx} e_s + \frac{\tau_{wsx}}{\rho_s'} - \frac{\tau_{bx}}{\rho_s'} \tag{11}$$

$$\frac{\partial q_{sy}}{\partial t} + \frac{\partial}{\partial x}\left(\frac{q_{sx} q_{sy}}{h_s}\right) + \frac{\partial}{\partial y}\left(\frac{q_{sy}^2}{h_s} + \frac{1}{2} g h_s^2 + g\chi h_w h_s\right) = g\chi h_w \frac{\partial z_s}{\partial y} - g(\chi h_w + h_s)\frac{\partial z_b}{\partial y} - \chi u_{wy} e_s + \frac{\tau_{wsy}}{\rho_s'} - \frac{\tau_{by}}{\rho_s'} \tag{12}$$

where $q_{wx} = u_{wx} h_w$, $q_{wy} = u_{wy} h_w$, $q_{sx} = u_{sx} h_s$, $q_{sy} = u_{sy} h_s$ are the unit discharges in the clear-water and the transport layer, respectively, in the direction x and y (for instance, the main-streamwise and transverse directions), respectively; (τ_{wsx}, τ_{wsy}), (τ_{sx}, τ_{sy}), and (τ_{bx}, τ_{by}) are the shear stresses on both sides of the interfaces and the ratio $\chi = \rho_w / \rho_s'$.

This shallow-water model is solved by a first-order finite-volume scheme on an unstructured triangular mesh (Toro 2001). A Riemann solver derived from the Harten-Lax-Van Leer formalism is used (Swartenbroekx et al. 2010a, Spinewine et al. 2011).

Bank-failure operator

The bank-failure operator consists in comparing locally for each computational cell the bed inclination α to the sediment critical angles α_c, considering the impact of a

water-level rise as a destabilizing phenomenon. After an erosion or deposition update due to the bed-load transport (equations 11-12), the unstable bed elements ($\alpha > \alpha_c$) are tilted around an appropriate axis of rotation, ensuring mass conservation of the assumed homogeneous material (Swartenbroekx et al. 2010b). The new inclination is imposed to a residual angle $\alpha = \alpha_r$. The critical and residual angles are distinct in submerged (subscript *s*) and emerged areas (subscript *e*).

As the set of equations (1) and (7-12) is solved using a first-order finite-volume model, each cell is assumed to have a unique sediment level. It is thus necessary to define the sediment level in each node in order to determine the cell slope, by preserving at the same time the sediment mass balance. The bank-failure algorithm can be summarised as follow:

Step 1: Update of the bed level z_b in the finite volume cells by the shallow-water model.

Step 2: Determination of the mean bed level in each apex of the cells to recover the continuity of the bed level. This process restores a continuous surface but affects the cell volume and thus the mass conservation that has to be recovered in turn.

Step 3: Subdivision of each main cell (with distinct bed levels at nodes) in three sub-cells, by adding an additional node at the centroid of the cell. The bed level in this new node is shifted vertically in order to ensure the sediment mass conservation between this main cell and the corresponding finite-volume cell. The main cell is now a pyramid whose three upper faces define three sub-cells

Step 4: Stability check in each main cell.

Step 5: Application of the bank-failure operator in each sub-cells of the unstable main cells. If a sub-cell slope overcomes the critical slope, the sub-cell upper face is tilted around an appropriate axis to allow the sub-cell to recover the residual angle, without affecting the mass conservation of all the cells and sub-cells affected by the shifting of the nodes implied in the tilting.

These Steps 4-5 are iterated until every cell is stable.

Step 6: Computation of the mean bed level z_b in each finite-volume cells in order to apply again the shallow-water model (Step 1).

Validation

To check the two-dimensional abilities of the numerical model, this is tested for a collapsing circular hole, under a constant water level at rest, but presenting unstable bank slopes. Then, the model is validated against laboratory tests of a dam-break flow; firstly in a prismatic channel made of coarse sand, and then over an initial bed step. The following parameters are used: $\rho_w = 1000$ kg/m³, $\rho_s' = 1369.6$ kg/m³, $C_s = 0.22$, $C_b = 0.53$, $\tau_{crit} = 0$ and $\varphi = 30°$.

Circular hole

A sand bed featuring a circular hole with a constant slope angle initially at 45° is submerged by 40 cm of water at rest (Figure 2a, grey line). The following parameters are imposed: $C_{fw} = 0.005$, $C_{fs} = 0.04$, $\alpha_{cs} = 35°$, $\alpha_{ce} = 87°$, $\alpha_{rs} = 30°$, $\alpha_{re} = 85°$. An average edge length of 5 mm is chosen for the triangular mesh.

In Figure 2b, where only a quarter of the hole is presented, it can be noticed that the model preserves the axial symmetry of the topography despite the unstructured triangular mesh.

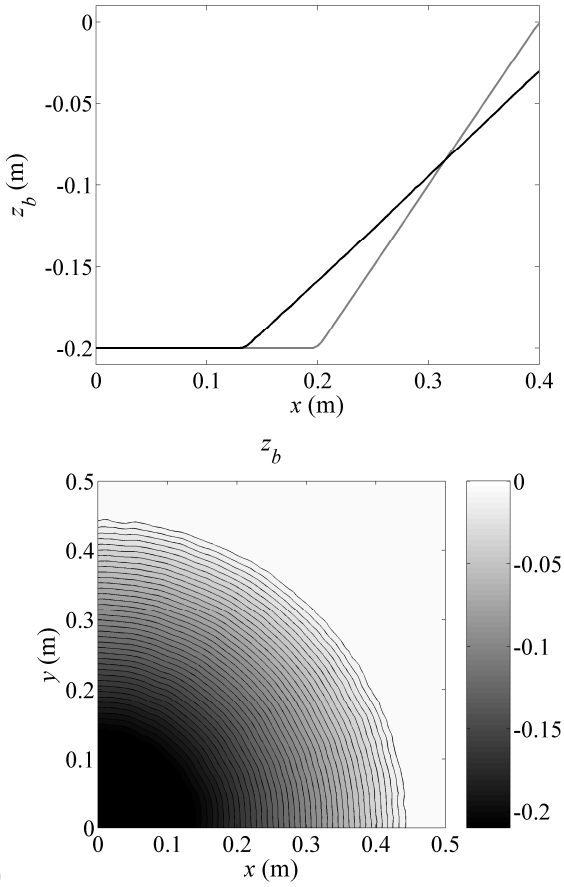

Figure 2: Circular hole topography: (a). Meridian section (grey) at t = 0 s and (black) at t = 60 s (b). Plan view at t = 60 s.

Dam-break wave in a prismatic channel

The model is tested for a dam-break flow in an initially half-channel of trapezoidal cross-section, whose dimensions are depicted in Figure 3 (Soares-Frazão et al. 2007). In this laboratory case, collapses of blocks of sand were observed. The following parameters are chosen:

$C_{fw} = 0.02$, $C_{fs} = 0.01$, $\alpha_{cs} = 35°$, $\alpha_{ce} = 87°$, $\alpha_{rs} = 30°$, $\alpha_{re} = 85°$. The average grid size is 1 cm.

In Figure 4, the agreement between the simulated and the measured topographies can be observed at two distinct cross-sections and three distinct times after the dam breaks. Too much deposition is predicted at $y = 0$ m at later time ($t = 10$ s, Figures 4e and 4f). However, except for this time, the profiles are in good accordance with the measured data. The root-mean-square-error (RMSE) of the predicted profiles compared to the measured one is given in Table 1.

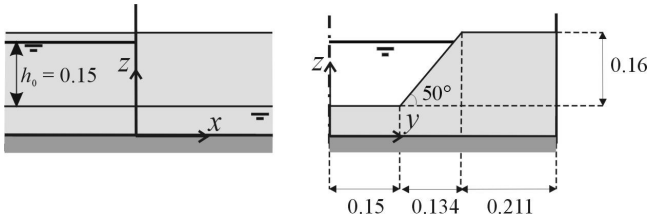

Figure 3: Initial conditions for the prismatic channel case.

Table 1: RMSE for bed levels associated with Figure 4

Figure 4	x (m)	t (m)	RMSE (m)
a	0.5	3	0.0106
b	1.5	3	0.0087
c	0.5	5	0.0135
d	1.5	5	0.0065
e	0.5	10	0.0138
f	1.5	10	0.0086

Dam-break wave over a movable bed step

The propagation of a dam-break wave over an initial downward sand bed step of 10 cm was simulated in the laboratory by Spinewine & Zech (2007). Figure 5 depicts the initial conditions. The following parameters are tested: $C_{fw} = 0.025$, $C_{fs} = 0.02$, $\alpha_{cs} = 15°$, $\alpha_{ce} = 87°$, $\alpha_{rs} = 10°$, $\alpha_{re} = 85°$. The average grid size is 1 cm.

Figure 6 and Figure 7 show the importance of the bank-failure operator to reproduce the dam-break wave: the step is almost not eroded without this operator (Figure 6, thick black lines) while the results are better with the operator (Figure 7, thick black lines). Except at first time $t = 0.25$ s (Figure 7a), when the shallow-water assumption is not yet valid, the wave front propagation and the transport layer thickness are rather well predicted. The root-mean-square-error (RMSE) of these profiles is given in Table 2.

Table 2: RMSE for the levels associated with Figure 7

Figure 7	Time t (s)	RMSE z_b (m)	RMSE z_s (m)	RMSE z_w (m)
a	0.25	0.0078	0.0055	0.0096
b	0.50	0.0056	0.0058	0.0074
c	0.75	0.0049	0.0055	0.0057
d	1.25	0.0048	0.0049	0.0089

Conclusions

A bank-failure operator is coupled to a 2D two-layer shallow-water model and tested against theoretical case and small-scale dam-break events on movable sand beds. The numerical model is solved on unstructured triangular meshes whose size could be locally adapted in complex geometries. The circular-hole test case has shown that no spurious directional effects are introduced by the numerical scheme. The model is able to simulate the bank collapse and the transverse slope evolution of a laboratory dam break in a prismatic channel. The capability of the model to treat also longitudinal unstable slope is also tested with the example of a dam-break wave on an initial bed step. The proposed model is able to predict both the progressive failure of the step and the bed-load wave.

References

Soares-Frazão,, S., le Grelle, N., Spinewine, B. & Zech, Y. (2007). Dam-break induced morphological changes with uniform sediments: measurements by a laser-sheet imaging technique. *Journal of Hydraulic Research*, IAHR, Vol. 45 Extra Issue, pp. 87-95.

Spinewine, B. and Zech, Y. (2007). Small-scale laboratory dam-break waves on movable beds. *Journal of Hydraulic Research*, IAHR, Vol. 45 Extra Issue, pp. 73-86.

Spinewine, B., Guinot, V., Soares-Frazão, S. and Zech, Y. (2011). Solution properties and approximate Riemann solvers for two-layer shallow flow models. *Computers & Fluids*; Vol. 44, pp. 202-220.

Swartenbroekx, C., Soares-Frazão, S., Spinewine, B., Guinot, V. and Zech, Y. (2010a). Hyperbolicity preserving HLL solver for two-layer shallow-water equations applied to dam-break flows. *Proceedings of River Flow 2010*, Braunschweig, Germany.

Swartenbroekx, C., Staquet, R., Soares-Frazão, S. and Zech, Y. (2010b). Two-dimensional operator for bank failures induced by water-level rise in dam-break flows. *Journal of Hydraulic Research*, IAHR, Vol. 48, No. 3, pp. 302-314.

Toro, E.F. (2001). *Shock-capturing methods for free-surface shallow flows*. Chichester: John Wiley & Sons, United Kingdom.

Zech, Y., Soares-Frazão, S., Spinewine, B., Savary, C. and Goutière, L. (2009). Inertia effects in bed-load transport models. *Canadian Journal of Civil Engineering*, Vol. 36, pp. 1587-1597.

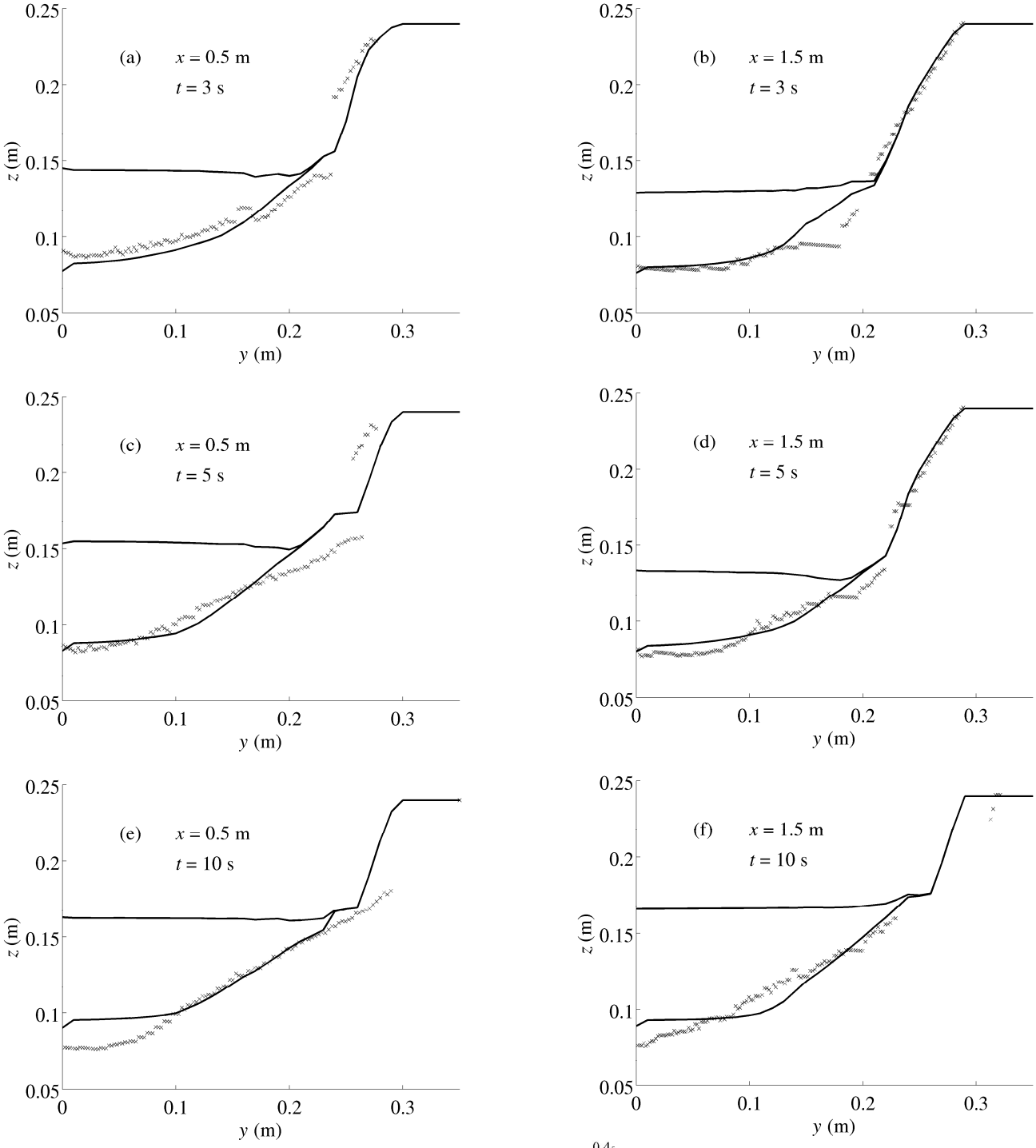

Figure 4: Water surface and bed cross-sections after the dam break, occurring at time $t = 0$ s. Measured data: grey crosses. Numerical model: black lines.

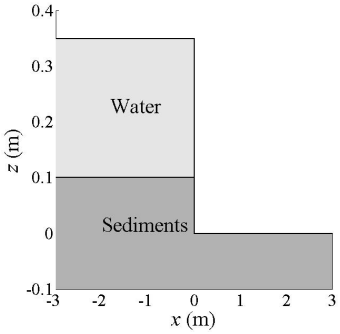

Figure 5: Initial conditions for the bed step: (dark grey) motionless bed, (light grey) clear water.

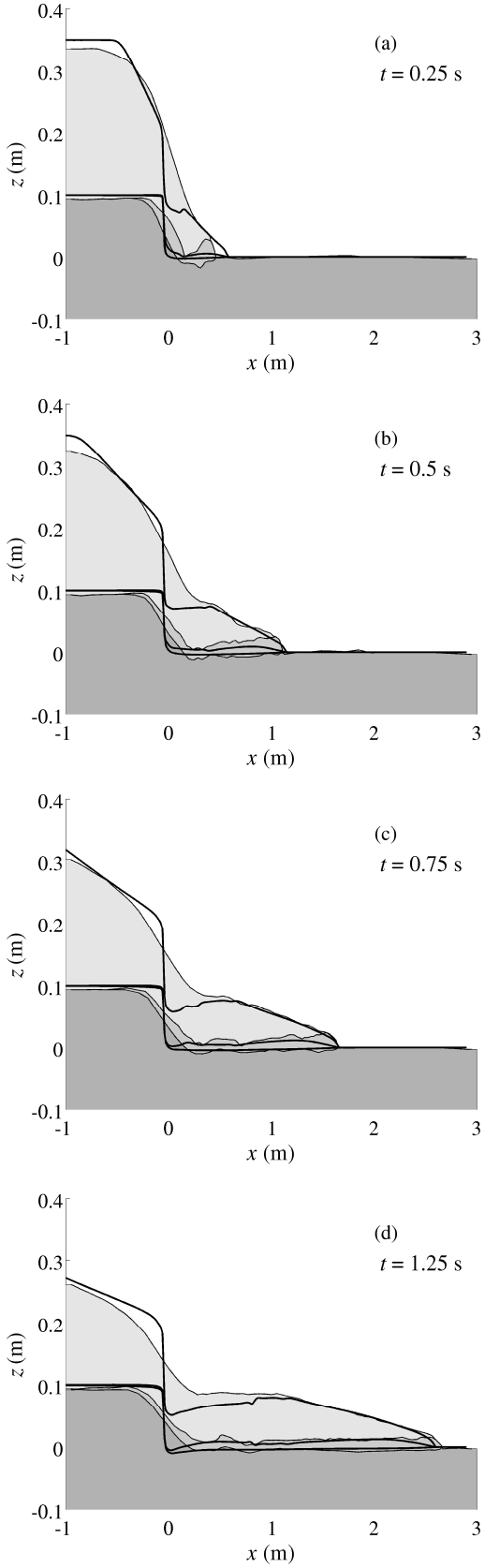

Figure 6: Longitudinal profiles for bed step. Experimental data: (dark grey) motionless bed, (medium grey) bed-load transport, (light grey) clear water. Numerical model: (thick black lines) without bank-failure operator.

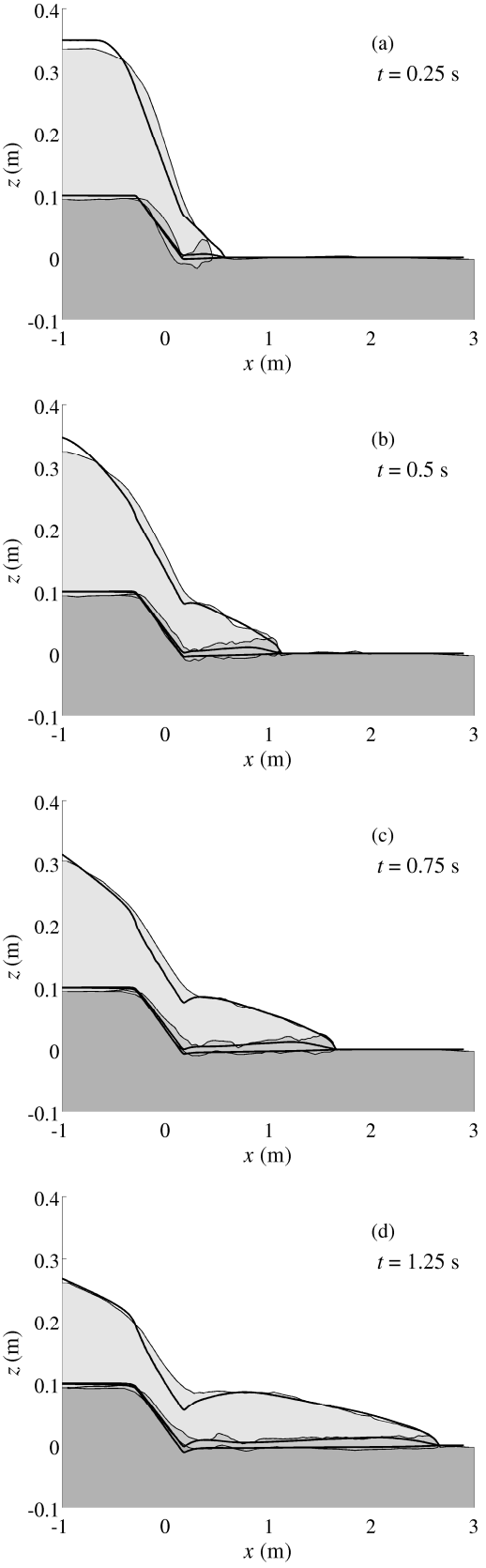

Figure 7: Longitudinal profiles for bed step. Experimental data: (dark grey) motionless bed, (medium grey) bed-load transport, (light grey) clear water. Numerical model: (thick black lines) with bank-failure operator.